Remote Sensing of Environment 221 (2019) 340–350

Contents lists available at ScienceDirect

Remote Sensing of Environment

journal homepage: www.elsevier.com/locate/rse

Proximal remote sensing of tree physiology at northern treeline: Do late-season changes in the photochemical reflectance index (PRI) respond to climate or photoperiod?

Jan U.H. Eitel[a,b,*], Andrew J. Maguire[a,b], Natalie Boelman[c,j], Lee A. Vierling[a,b], Kevin L. Griffin[c,d,j], Johanna Jensen[d], Troy S. Magney[e], Peter J. Mahoney[f], Arjan J.H. Meddens[a], Carlos Silva[g,h], Oliver Sonnentag[i,k]

[a] Department of Natural Resources and Society, College of Natural Resources, University of Idaho (UI), 875 Perimeter Drive, Moscow, ID 83843, USA
[b] McCall Outdoor Science School, College of Natural Resources, University of Idaho, 1800 University Lane, McCall, ID 83638, USA
[c] Lamont-Doherty Earth Observatory, Columbia University, Palisades, NY 10964, USA
[d] Department of Ecology, Evolution and Environmental Sciences, Columbia University, New York, NY 10027, USA
[e] Jet Propulsion Laboratory, California Institute of Technology, Pasadena, CA, USA
[f] School of Environmental and Forest Sciences, University of Washington, Seattle, WA, USA
[g] Biosciences Laboratory, NASA Goddard Space Flight Center, Greenbelt, MD 20707, USA
[h] Department of Geographical Sciences, University of Maryland, College Park, MD 20740, USA
[i] Département de Géographie, Université de Montréal, Montréal, QC, Canada
[j] Department of Earth and Environmental Sciences, Columbia University, Palisades, NY 10964, USA
[k] Centre D'Études Nordiques, Université de Montréal, Montréal, QC, Canada

ARTICLE INFO

Keywords:
Forest Tundra Ecotone
Northern treeline
MODIS
Photoperiod
PRI
Solar radiation
Climate change
Photosynthetic phenology

ABSTRACT

Relatively little is known of how the world's largest vegetation transition zone – the Forest Tundra Ecotone (FTE) – is responding to climate change. Newly available, satellite-derived time-series of the photochemical reflectance index (PRI) across North America and Europe could provide new insights into the physiological response of evergreen trees to climate change by tracking changes in foliar pigment pools that have been linked to photosynthetic phenology. However, before implementing these data for such purpose at these evergreen dominated systems, it is important to increase our understanding of the fine scale mechanisms driving the connection between PRI and environmental conditions. The goal of this study is thus to gain a more mechanistic understanding of which environmental factors drive changes in PRI during late-season phenological transitions at the FTE – including factors that are susceptible to climate change (i.e., air- and soil-temperatures), and those that are not (photoperiod). We hypothesized that late-season phenological changes in foliar pigment pools captured by PRI are largely driven by photoperiod as opposed to less predictable drivers such as air temperature, complicating the utility of PRI time-series for understanding climate change effects on the FTE. Ground-based, time-series of PRI were acquired from individual trees in combination with meteorological variables and photoperiod information at six FTE sites in Alaska. A linear mixed-effects modeling approach was used to determine the significance ($\alpha = 0.001$) and effect size (i.e., standardized slope b*) of environmental factors on late-seasonal changes in the PRI signal. Our results indicate that photoperiod had the strongest, significant effect on late-season changes in PRI ($b^* = 0.08$, $p < 0.001$), but environmental variables susceptible to climate change were also significant (i.e., daily mean solar radiation ($b^* = -0.03$, $p < 0.001$) and daily mean soil temperature ($b^* = 0.02$, $p < 0.001$)). These results suggest that interpreting PRI time-series of late-season phenological transitions may indeed facilitate our understanding of how northern treeline responds to climate change.

* Corresponding author at: Department of Natural Resources and Society, College of Natural Resources, University of Idaho (UI), 875 Perimeter Drive, Moscow, ID 83843, USA.
E-mail address: jeitel@uidaho.edu (J.U.H. Eitel).

https://doi.org/10.1016/j.rse.2018.11.022
Received 22 June 2018; Received in revised form 30 October 2018; Accepted 17 November 2018
Available online 27 November 2018
0034-4257/

1. Introduction

The Forest Tundra Ecotone (FTE) is the world's largest ecological transition zone spanning 13,400 km across the northern hemisphere (Callaghan et al., 2002). This vast circumpolar transition zone between the boreal forest and the Arctic tundra is experiencing warming more rapidly than any other ecoregion on earth (Kattsov et al., 2005; Serreze et al., 2000). Potential changes in the FTE could have far reaching consequences for global biogeochemical cycling (Zhang et al., 2013), regional energy balance (Harding et al., 2002), biodiversity of flora and fauna (Skre et al., 2002), as well as ecosystem services and socio-economics of Arctic-Boreal regions (Callaghan et al., 2002) – yet, relatively little is known about how the FTE is responding to warming.

A promising approach for improved understanding of the effects of climate change on inaccessible vegetation in the FTE is the study of seasonal changes in photosynthesis, or "photosynthetic phenology". To track photosynthetic phenology at the landscape scale, many studies have been relying on time-series of spectral indices that can be derived from satellite imagery (e.g., Reed et al., 1994; Zeng et al., 2011; Jeong et al., 2011; Piao et al., 2011; Wang et al., 2015; Park et al., 2016). The spectral indices used by these studies (e.g., the Normalized Difference Vegetation Index or NDVI; EVI or the Enhanced vegetation index) employ parts of the electromagnetic spectrum that are sensitive to changes in leaf area and to a much lesser degree changes in leaf pigment pools (e.g., Eitel et al., 2011; Gamon et al., 1995). Consequently, these indices mainly track seasonal transitions in deciduous plant-assemblages associated with leaf development in the spring and leaf-abscission during late-season which closely track changes in photosynthetic phenology (e.g., Gamon et al., 1995). However, much of the FTE is dominated by evergreen species such as white spruce (*Picea glauca*) and or black spruce (*Picea mariana*) characterized by negligible seasonal changes in leaf area. This limits the use of these spectral indices for remotely tracking photosynthetic phenology. To overcome this limitation, spectral vegetation indices could be used that are sensitive to seasonal changes in pigment pools. These changes are controlled by a complex interaction between genetics and environmental factors such as photoperiod, temperature and incident light (Niinemets et al., 2003; Heide, 1974; Salisbury, 1981; Thomas and Vince-Prue, 1997; Rosenthal and Camm, 1997; Busch et al., 2008; Cooke et al., 2012; Ensminger et al., 2015).

The complex interaction between genetics and environmental factors may be particularly important to consider at the FTE where harsh growth conditions may have caused unique evolutionary adaptations with important implications on which of these environmental factors control changes in pigment pools and to what degree (Howe et al., 2003; Tang et al., 2016). In particular, relying on photoperiod as a deterministic signal to control changes in chlorophyll carotenoid ratios could be advantageous as opposed to relying on more stochastic environmental controls such as air temperature. An increase in the latter may temporarily increase carbon gain but at the same time would pose excessive physiological risk (e.g., to a sudden late-season freeze event) for trees at the FTE where drastic weather shifts are common (Körner, 2012; Körner et al., 2016).

Physiologically, changes in pigment pools enable plants to adapt their light use efficiency (LUE) to changing environmental conditions to optimize carbon gain during suitable growth conditions while minimizing the likelihood of damage to their photosystems (Adams and Demmig-Adams, 1994; Adams and Demmig-Adams, 1995; Adams et al., 2002; Adams et al., 2004; Verhoeven, 2014). Seasonal changes in LUE occur primarily via shifts in the relative pool sizes of chlorophyll and carotenoid pigments. Chlorophyll pigments absorb light that provides the energy needed to drive photosynthesis, and as such, chlorophyll concentration tends to be higher during the growing season when warm temperatures enable catalyzed reactions to occur, and lower outside of the growing season when temperatures and/or light limit/inhibit photosynthetic activity (Sofronova et al., 2016). Carotenoid pigments, including xanthophylls and carotenes, play an important role in dissipating excess light energy as heat (i.e., thermal dissipation) to avoid damage to the photosystems. Thus, seasonal shifts in ratios of chlorophyll to carotenoid pools offers an important photoprotective mechanism by which plants can regulate the absorption and dissipation of incoming energy. We contend this is likely particularly important for plants in the FTE during spring and late-season when temperatures are often too low for photosynthetic activity, yet the light environment is often extreme due to long days (12+ hours of daylight), high albedo of snow amplifying solar irradiance, and sparse canopy cover limiting shade (Tranquillini, 1979).

To remotely detect seasonal changes in the ratios of chlorophyll to carotenoid pools, the photochemical reflectance index (PRI) has been used (Wong and Gamon, 2015b). This spectral vegetation index is sensitive to plant physiological processes and relies on reflectance values at 531 nm and 570 nm. The 531 nm wavelength falls in the absorption region of both chlorophyll and carotenoids, whereas only chlorophyll absorbs the incoming light at 570 nm (Gamon et al., 1992, 1997). Hence, PRI is sensitive to seasonal changes in the ratio of chlorophyll to carotenoid concentrations. However, it is also sensitive to diurnal variations in the concentration of xanthophyll cycle pigments which make up a portion of the total carotenoid pool (Garrity et al., 2011; Gamon et al., 2016; Filella et al., 2009; Wong and Gamon, 2015a). Over seasonal timescales, chlorophyll to carotenoid ratios have been shown to dominate the diurnal signal caused by light induced changes of xanthophyll-cycle pigments (Filella et al., 2009; Porcar-Castell et al., 2012; Fréchette et al., 2016; Gamon et al., 2015) making it a promising index for tracking photosynthetic phenology in evergreen species (Wong and Gamon, 2015a, b). For example, work by Wong and Gamon (2015b) showed that PRI from ground-based reflectance measurements closely tracked the onset of photosynthetic activation in evergreen conifer seedlings.

Despite these recent findings, the availability of satellite derived PRI time-series to study photosynthetic phenology at the FTE has been limited. This recently changed for North America and Europe when NASA made available a 16-year time-series of multi-angle implementation of atmospheric correction (MAIAC) processed MODIS data (https://e4ftl01.cr.usgs.gov/MOTA/; Lyapustin et al., in review). These atmospherically corrected datasets of surface reflectance allow PRI to be calculated using a green band centered around 531 nm (band 11, 526–536 nm) and a red reference band (band 1, 620–670 nm). Gamon et al. (2016) demonstrated that a MODIS derived version of PRI - the Chlorophyll Carotenoid Index (CCI) – tracked seasonal changes in photosynthetic carbon uptake at sites dominated by conifer species including eastern hemlock (*Tsuga canadensis*), red spruce (*Picea rubens*), loblolly pine (*Pinus taeda*), Douglas fir (*Pseudotsuga menziesii*) and western hemlock (*Tsuga heterophylla*). Similarly, Ulsig et al. (2017) showed promising relationships ($R^2 = 0.80$) between the start of the growing season in Scots pine (*Pinus sylvestris*) determined by ground-based flux tower measurements of net ecosystem exchange (NEE) and MODIS derived PRI time-series.

The results from the above research by Gamon et al. (2016) and others (e.g., Ulsig et al., 2017; Middleton et al., 2016) suggest that PRI-based vegetation indices may reveal links between environmental variables and photosynthetic phenology. The goal of this study is to gain a more mechanistic understanding on which environmental factors drive changes in PRI at the FTE during late-season phenological transitions – including those susceptible to climate change (e.g., air- and soil temperature) and those not susceptible to climate change (e.g., photoperiod) – and the degree to which these relationships exist. We hypothesized that gradual late-season phenological changes captured by PRI are largely driven by changes in photoperiod as opposed to more stochastic drivers such as temperature. Support for this hypothesis would limit the suitability of late-seasonal PRI time-series for understanding climate change effects on the FTE.

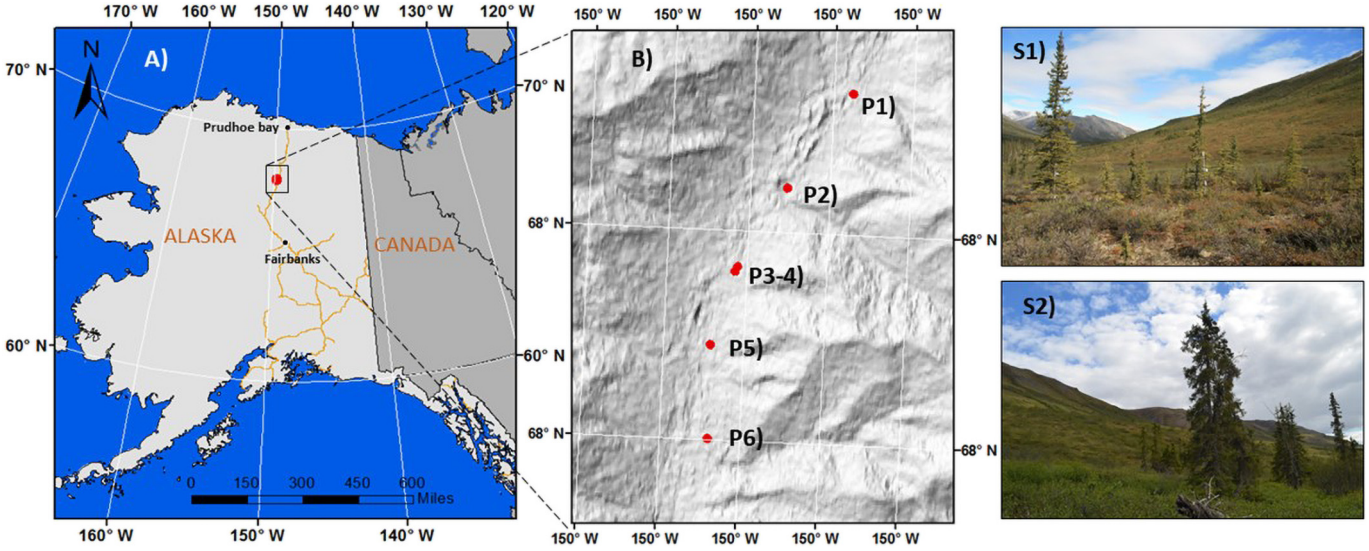

Fig. 1. Map of the study area. A) Alaska; B) hillshade map of the six study plots; P1–P6) profile view of two study plots. The orange line represents primary and secondary roads. Red dots represent the location of the study plots. (For interpretation of the references to colour in this figure legend, the reader is referred to the web version of this article.)

2. Materials and methods

2.1. Study area

Field data were collected during the late-growing season (June 30th–September 20th) in 2016 and 2017 along an approximately 5.5 km long south-north transect across the FTE near the Dalton Highway (67°59′ 40.92″ N latitude, 149°45′ 15.84″ W longitude), Alaska, USA (Fig. 1). There, trees are increasingly sparse and the landscape eventually transitions into treeless tundra. Along this transect, six study plots (P1 to P6, see Fig. 1) were established, each with six study trees:three with diameter at breast height (dbh; cm at 1.37 m above ground) ≥10 cm and three with dbh < 10 cm, resulting in a total of 36 study trees. The tree characteristics for each plot are summarized in Table 1. Mean annual precipitation and air temperature for the study area as measured at a nearby SnowTelemetry (SNOTEL) site between 2007 and 2016 was 48.54 cm and −8.12 °C, respectively (https://wcc.sc.egov.usda.gov/nwcc/site?sitenum=957). The FTE is underlain by continuous permafrost and consists of white spruce (*Picea glauca* (Moench) Voss) with sedges (e.g., *Eriophorum* spp.) and low-stature deciduous shrubs (e.g., *Betula nana* L., *Alnus* spp.) in the understory.

Table 1
Summary of tree characteristics for each of the six study plots: diameter at breast height (dbh), tree height, dripline area, and canopy openness. Tree height and dripline area were derived from terrestrial lidar data. Canopyopenness was determined based on hemispherical photographs taken at all four cardinal directions with a digital camera (CoolPix 4500, Nikon Corporation, Tokyo Japan) equipped with a fisheye lens.

Plot	Diameter at breast height (cm)	Tree height (m)	Dripline area (m^2)	Canopy openness (%)
	Mean (sd)	Mean (sd)	Mean (sd)	Mean (sd)
1 (n = 6)	12.52 ± 7.32	5.64 ± 2.47	3.31 ± 2.11	0.23 ± 0.06
2 (n = 6)	10.07 ± 6.00	6.13 ± 3.58	1.77 ± 1.24	0.18 ± 0.03
3 (n = 6)	10.02 ± 4.70	6.23 ± 2.40	2.27 ± 1.64	0.19 ± 0.03
4 (n = 6)	13.33 ± 7.47	7.80 ± 4.08	2.50 ± 1.69	0.23 ± 0.02
5 (n = 6)	13.93 ± 6.20	8.65 ± 3.70	3.23 ± 1.39	0.20 ± 0.02
6 (n = 6)	9.99 ± 4.56	6.03 ± 2.83	1.83 ± 1.09	0.21 ± 0.04
All (n = 36)	11.64 ± 5.94	6.75 ± 3.20	2.49 ± 1.57	0.21 ± 0.04

2.2. Field data

2.2.1. Acquisition of photochemical reflectance index (PRI) time-series and processing

Canopy reflectance measurements centered at 532 and 570 nm were collected at each of the 36 tree locations in 5-minute sampling intervals using rugged spectral reflectance sensors (SRS, METER, Pullman, WA). These spectrally calibrated optical sensors allow for autonomous measurement of reflectance at both PRI wavelengths by making use of a hemispherical up-looking and down-looking (field-stop) sensor that measures incoming and upwelling radiation, respectively (after Garrity et al., 2010, Gamon et al., 2015, and Magney et al., 2016). The peak sensitivity of both the hemispherical and field-stop sensor is centered at 532 nm and 570 nm with a 10 nm full-width half-maximum band width. To correct for cosine effects on measured radiation, the hemispherical sensor is equipped with a Teflon diffuser. The field-stop PRI sensors were equipped with an interference filter restricting the field of view to 20°. Further details on the SRS sensor can be found here: http://manuals.decagon.com/Manuals/14597_SRS_Web.pdf

At each of the 36 tree locations, a hemispherical and field-stop PRI sensor were installed within the tree canopy on the south facing side of the tree approximately 1.5 m above ground, ensuring that the field-of-view (FOV) of the field-stop sensor was dominated by the study tree's foliage. Both the hemispherical and field-stop PRI sensor were installed directly adjacent to each other with a nadir viewing angle for the field stop PRI sensor and a sky looking view zenith angle of 180° for the hemispherical PRI sensor.

From the SRS-provided spectral measurements, a mean PRI was calculated for each day at constant solar zenith angle (solar zenith angle between 80° and 90°) hereafter referred to as PRI_0:

$$PRI_0 = (R_{532nm} - R_{570nm})/(R_{532nm} + R_{570nm}) \quad (1)$$

where R_{532nm} and R_{570nm} are the reflectance values measured at 532 nm and 570 nm, respectively, and the daily timing of the constant solar zenith angle was determined using the R insol package (Corripio, 2014). PRI values included in the calculation of the mean were limited to solar zenith angles occurring in the early morning and late evening to (i) minimize variations in PRI due to midday variation in light intensity that are known to affect PRI due to variations in xanthophyll cycle pigments (Gamon et al., 1992; Demmig-Adams and Adams, 1992) and (ii) to minimize potentially confounding bidirectional reflectance

distribution function (BRDF) effects on PRI readings (Middleton et al., 2009). Because the fraction of diffuse to direct irradiance is relatively higher at high solar zenith angles found during early morning and late evening twilight, and because our field site is situated in a valley (Fig. 1B) such that the solar disk is also blocked by mountains during these periods, vegetation receives nearly directionally uniform, or 'flat field' irradiance during these periods. As a result, BRDF effects are less pronounced in the early morning and evenings. Smaller PRI_0 values are associated with lower chlorophyll to carotenoid ratios, while larger PRI values are associated with higher chlorophyll to carotenoid ratios (Boelman et al., 2016).

2.2.2. Physical growth environment

To characterize fine-scale variations in the physical growth environment, the following micrometeorological variables were measured in 5-minute sampling intervals at each of the 36 tree locations: air temperature (Ta in °C), soil temperature (Ts in °C), vapor pressure deficit (VPD in Pa), and solar radiation (SR in $W\,m^{-1}$). A meteorological monitoring sensor equipped with a radiation shield (VP-4, METER, Pullman, WA) was used to measure Ta and VPD. The sensor was installed near the PRI sensors while ensuring that it did not interfere with PRI measurements. To characterize the local light environment of the spectrally monitored part of the canopy, SR was approximated based on hemispherical PRI data. For this, SR (PYR Solar Radiation Sensor, METER, Pullman, WA) and hemispherical PRI data were simultaneously collected at one location directly adjacent to each other and a calibration equation was fit between the measured SR and the data collected by the hemispherical PRI sensor at 531 nm. The resulting linear calibration equation ($SR = 1.9446 + 551.32 * x$, $r^2 = 0.92$) was then applied to data collected by the hemispherical PRI sensor at 531 nm to get proxies of the local light environment viewed by the PRI sensors at each study tree. The soil temperature was measured with a rugged temperature sensor (RT-1, METER, Pullman, WA) at 10 cm depth (following Körner, 2012) on the northern side of each of the 36 study trees below the canopy dripline.

To summarize each of the variables for a given day, the following daily summary statistics were calculated for each of the variables: mean, maximum (max), minimum (min), and standard deviation (sd). From the air temperature data, we further calculated daily growing degree days (GDD) using the following equation with a base air temperature of 5 °C (Sykes et al., 1996; Ramankutty et al., 2002):

$$GDD = ((Ta_{max} + Ta_{min})/2) - 5^{\circ} \quad (2)$$

If Ta_{min} was less than the base air temperature of 5 °C, a GDD value of 0 was recorded. Photoperiod was determined based on the geographic location of the study sites and date using the insol package (Corripio, 2014) in R (R Core Team, 2017).

2.2.3. Needle pigments

Between 2 and 4 branches were collected in mid-July and late September of 2017 from each of 6 of the 36 trees for which PRI and physical growth environment variables were measured. All branches sampled were chosen subjectively to ensure that only sun exposed needles were chosen from each tree. For the transport back to the laboratory, branches were wrapped in wet paper towel and foil, kept in a cooler with ice until pigment extraction began within 3 h after collection. If not processed within 3 h, branch samples were frozen until pigment extraction. Between 5 and 10 needles from the previous yearwere removed from each branch, so that all pigment and associated values could be calculated per branch sample. Both wet weight and needle area were measured prior to pigment extraction. To extract pigments, needles were first cut into fine pieces ($< 1\ mm^2$) and ground rapidly with a mortar and pestle in 100% acetone (with small amounts of sand to aid with grinding, $MgCO_3$ to prevent acidification, and ascorbic acid to prevent degradation of pigments) until no green needle fragments remained. Pigment extracts were then centrifuged, diluted, and the absorbance of the supernatant was measured at 470, 645, 662 and 710 nm with a visible spectrophotometer (Go Direct SpectroVis Plus Spectrophotometer, Vernier, OR, USA). Pigment pool sizes quantified were chlorophyll *a* (Chl*a*), chlorophyll *b* (Chl*b*), and bulk carotenoids (Car) (in ug/cm^2), which were calculated with coefficients determined by Lichtenthaler, 1987. The Chl*a* and Chl*b* values were combined to calculate the total chlorophyll pool size (Chl = Chl*a* + Chl*b*). The pigment ratio in Chl:Car was also calculated.

2.3. Data analysis

Observations collected from 18 of 36 trees were removed from the analysis from the 2016 dataset (final n = 18) and an additional 8 trees from the 2017 dataset (final n = 10) because i) sensor cables were damaged by small mammals, resulting in incomplete datasets and ii) permafrost thaw caused the movement of an individual PRI sensor FOV away from the originally monitored foliage and thus resulting in a drastic shift in the reflectance signal. We also removed observations during which snow was present at the study sites due to their potential confounding effects on the PRI signal (e.g., Ulsig et al., 2017). Time-lapse photography from the study sites was used to determine days during which snow was on the ground. The final dataset used for statistical analysis had a total of 2060 individual PRI and explanatory variable observations (1290 observations in 2016 and 770 in 2017).

To determine the effect of environmental factors on PRI_0, a linear mixed effects analysis was performed with the statistical software R (R Core Team, 2017) using the 'nlme' package (Pinheiro et al., 2017) with PRI_0 as the dependent variable, environmental variables and year as fixed effects, and tree and plot identification number as nested random effects. From this full model consisting of 18 predictor variables (GDD, photoperiod, and daily summary statistics of Ta, Ts, VPD, and SR), the predictor variable with the highest variance inflation factor (VIF) was removed in a step-wise process until all predictor variables had a VIF of < 3 (Zuur et al., 2010). All input variables were standardized by two standard deviations (Gelman, 2008). In order to evaluate the temporal structure in residuals associated with longitudinal data, models with and without temporally autocorrelated errors were contrasted using Akaike information criterion (AIC; Akaike, 1974). Given the relatively simple trend in PRI_0 (Fig. 2), only first-order autoregressive and autoregressive-moving-average models were considered. The p-values associated with each of the predictor variables in the best model (i.e., lowest AIC) were calculated based on the Wald-statistics approximation implemented in the 'sjPlot' package (Lüdecke, 2018). We considered predictor variables at $p < 0.001$ to be statistically significant and used the standardized slope (b*) to determine the effect size of each predictor variable (Schielzeth, 2010). Assumptions of normality were evaluated using residual diagnostics and quantile-quantile plots in both fixed and random effects (Zuur et al., 2010).

3. Results

3.1. Time-series of environmental variables and PRI_0

The time-series of the collected environmental data varied along a general late-season-seasonal trend though there were distinct differences in their progression between the two years (Fig. 2). For instance, Ta_{mean} showed pronounced differences between 2016 and 2017; July and August Ta_{mean} temperatures were warmer in 2017 but considerably colder than in 2016 between mid-August to early September. This trend reversed again through much of September when growing season temperatures in 2017 were noticeably higher than in 2016. Further, Ts_{mean} increased in early July during both years before oscillating; however, the pronounced and lasting drop in soil temperature occurred much later in 2016 (early September) when compared to 2017 (mid August). The pooled PRI_0 data from all trees showed a statistically significant decrease ($p < 0.0001$) from the peak of the growing season

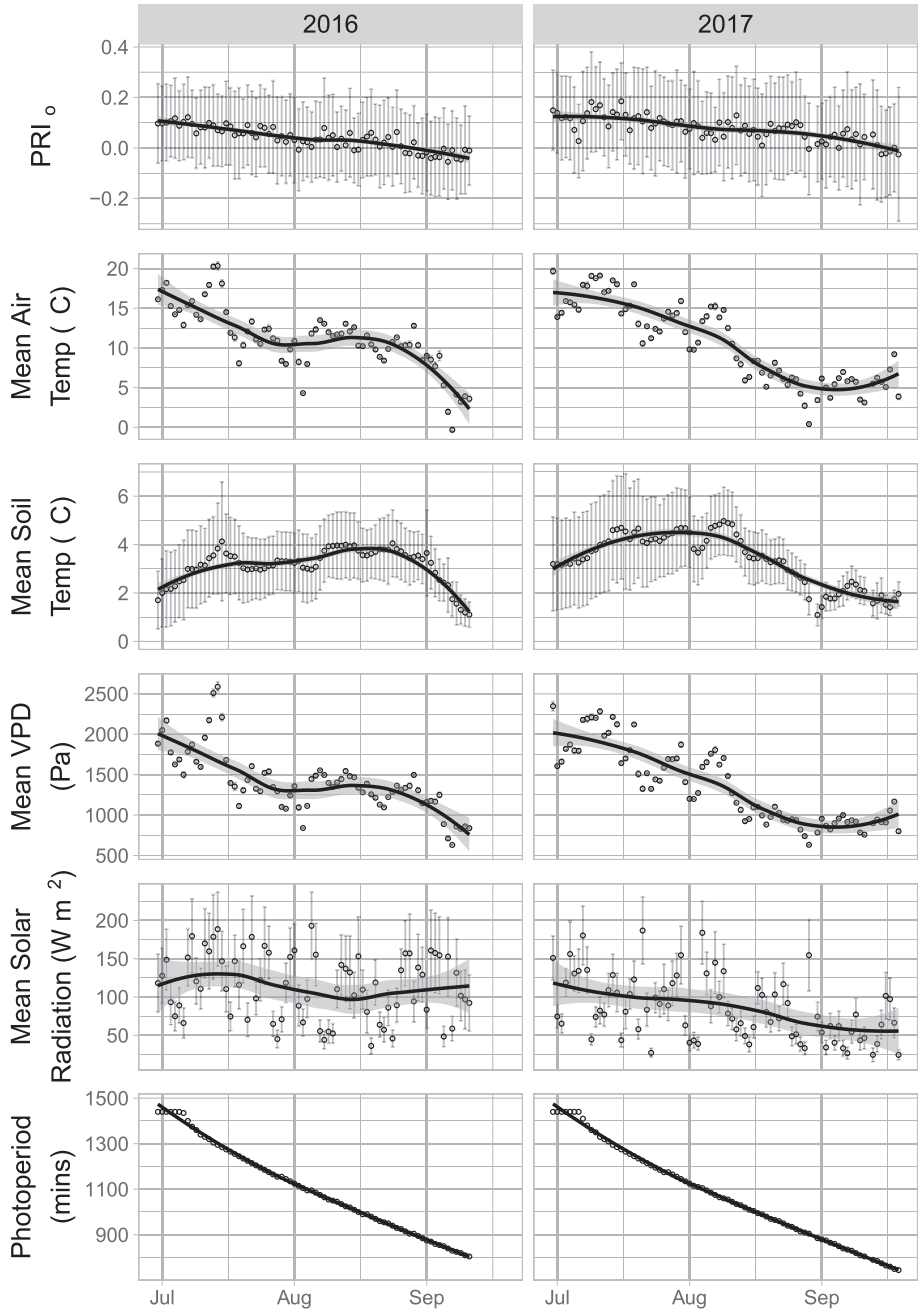

Fig. 2. Late-season trends for: PRI_0, mean air temperature (Ta_{mean}), mean soil temperature (Ts_{mean}), mean vapor pressure deficit (VPD_{mean}), mean solar radiation (SR_{mean}), and photoperiod observed for all trees studied between June 30th and September 20th 2016 (n = 18) and 2017 (n = 10). Error bars indicate one standard deviation and to aid visual interpretation smoothing curves with confidence intervals (grey area) were added using the loess function in R (R Core Team, 2017).

to the end of the growing season (Fig. 3). This decrease is mirrored by a statistically significant decrease ($p < 0.0001$) in chlorophyll to carotenoid ratios (Fig. 4), similar to previous studies showing a decrease in chlorophyll to carotenoid ratios from the peak of the growing season to the end of the growing season (e.g., Sofronova et al., 2016; Bowling et al., 2018). Timeseries of PRI_0 are different between years, which might be partly explained by changes in sample size between years (see Section 2.3 Data analysis), but also by inter-annual differences in environmental conditions. Average PRI_0 values for both 2016 and 2017 (Fig. 3) are relatively high when compared to PRI readings shown in other studies (e.g., Garbulsky et al., 2011; Wong and Gamon, 2015a, b; Magney et al., 2016) suggesting that observed trees experienced limited environmental stress under low early morning and late evening light conditions.

Declines in PRI_0 over the course of the late-season sampling period warranted consideration of temporal patterns in model residuals per the assumptions of linear regression. An evaluation of the time-series residuals indicated small but important patterns in the error structure indicative of temporal autocorrelation. Specifically, AIC supported a first-order autoregressive-moving-average error structure that was able to correct the problematic autocorrelation in the final linear mixed effects model (Fig. S1 in Supp. data).

3.2. Effects of environmental variables on PRI_0

After excluding highly collinear predictor variables based on VIF values, a linear mixed effects model was fit with Ta_{sd}, Ts_{mean}, Ts_{max}, photoperiod, and SR_{mean} as fixed effects on PRI_0. The model was fit with

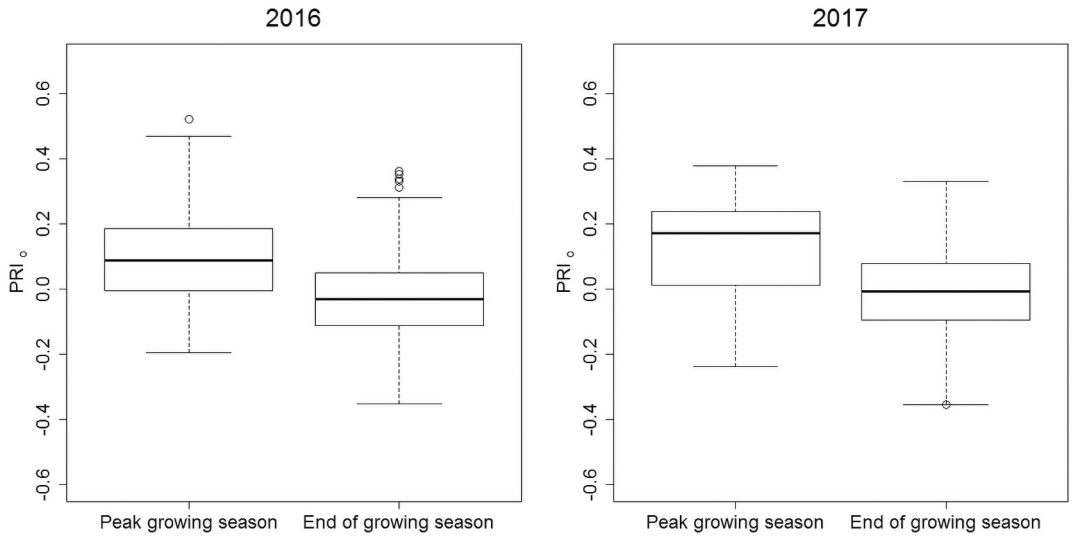

Fig. 3. Changes in PRI_0 between the peak of the growing season to the end of the growing season for 2016 and 2017. Boxes display the first quartile, median, and third quartile, whiskers display the range of each sample plot. Individual points represent outliers that are 1.5 times greater than the 75th percentile.

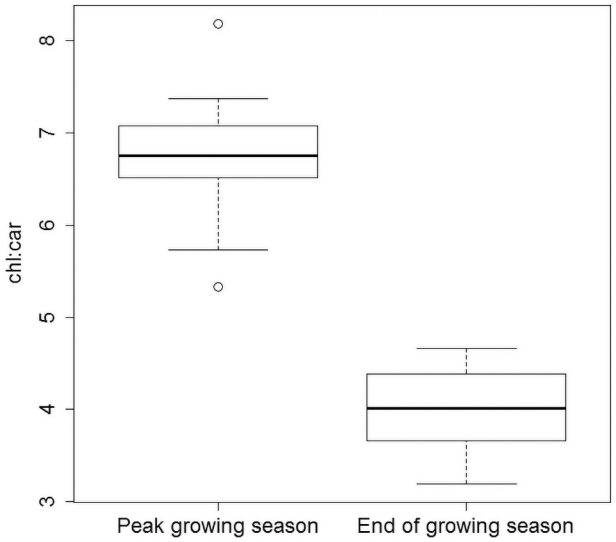

Fig. 4. Changes in chlorophyll carotenoid ratios between the peak of the growing season to the end of the growing season. Data only available for 2017. Boxes display the first quartile, median, and third quartile, whiskers display the range of each sample plot. Individual points represent outliers that are 1.5 times greater than the 75th percentile.

and without interaction terms, but based on a likelihood ratio test, interactions did not significantly improve model performance and hence no interactions were included in the final model. The results from the linear mixed effects model reveal that photoperiod has decidedly the strongest (b* = 0.08) significant effect on the PRI_0, followed by SR_{mean} (b* = −0.03) and Ts_{mean} (b* = 0.02) (Figs. 5 and 6).

Even though their respective effect sizes are considerably lower than that of photoperiod, SR_{mean} (b* −0.03) and Ts_{mean} (b* 0.02) also showed statistically significant effects on PRI_0. The negative standardized slope estimate for SR_{mean} in the mixed effects model (Fig. 5) suggests a negative relationship between PRI_0 and SR_{mean}, generally agreeing with previous work on broadleafed trees where chlorophyll decreased with increasing quantum flux density while xanthophyll pigments were relatively unaffected resulting in a negative relationship between available light and the ratio between chlorophyll and xanthophyll cycle carotenoids (Niinemets et al., 2003).

4. Discussion

4.1. Environmental controls of temporal variation in late-season PRI_0 time-series

The results of this study partly support our hypothesis that trees at the FTE predominantly rely on a deterministic photoperiod signal to drive pigment pool changes in the late-season that is largely unaffected by intra- and inter-seasonal variability in environmental variables (Fig. 5). The physiological explanation for this is likely that enhanced sensitivity to more intra-seasonally variable environmental signals such as Ta might pose excessive physiological risk for trees at the FTE where weather conditons are extreme and drastic weather shifts are common (Körner, 2012). An example of drastic weather swings shown in this study is around mid-July of 2016 when Ta_{mean} dropped from around 20 °C to 8 °C within 5 days (Fig. 2). To survive these extreme weather conditions, trees at the FTE have likely evolutionarily adapted so their photosynthetic phenology is mostly responsive to stable signals such as photoperiod rather than more stochastic signals from environmental variables such as Ta. Such evolutionary adaptations of phenology have been documented along latidudinal and elevational gradients where growth conditons are becoming more extreme at the highest latitudes and elevations (Vaartaja, 1954; Heide, 1974; Dormling et al., 1968; Körner et al., 2016). For example, in a controlled experiment with Norway spruce (*Picea abies*), Heide (1974) showed distinct differences in critical photoperiods between ecotypes with apical growth ceasing earlier (i.e., longer critical photoperiod) in higher latitudinal and elevational ecotypes. In another study (Malcolm and Pymar, 1975), both northern and southern provenances of Sitka spruce (*Picea sitchensis*) exhibited cessation of shoot extension at a photoperiod of 16 h when exposed to cooler temperature treatments (day/night: 12/7 °C and 8/5 °C). In contrast, under warm temperature treatments (day/night: 20/11 °C and 16/9 °C), southern provenances continued shoot extension until photoperiod declined to 12 h whereas northern provenances stopped growing at a photoperiod of 15.5 h, approximately the same photoperiod as under cool temperature treatment, irrespective of the warming treatments.

Though their effect was demonstrably smaller when compared to photoperiod, both SR_{mean} and Ts_{mean} also exhibited significant controls on PRI_0 suggesting that these envirommental factors interact with photoperiod and enable modulation of pigment pools during the late-season transition (Figs. 5 and 6). This finding is in broad agreement with previous findings showing the interactive effects of photoperiod

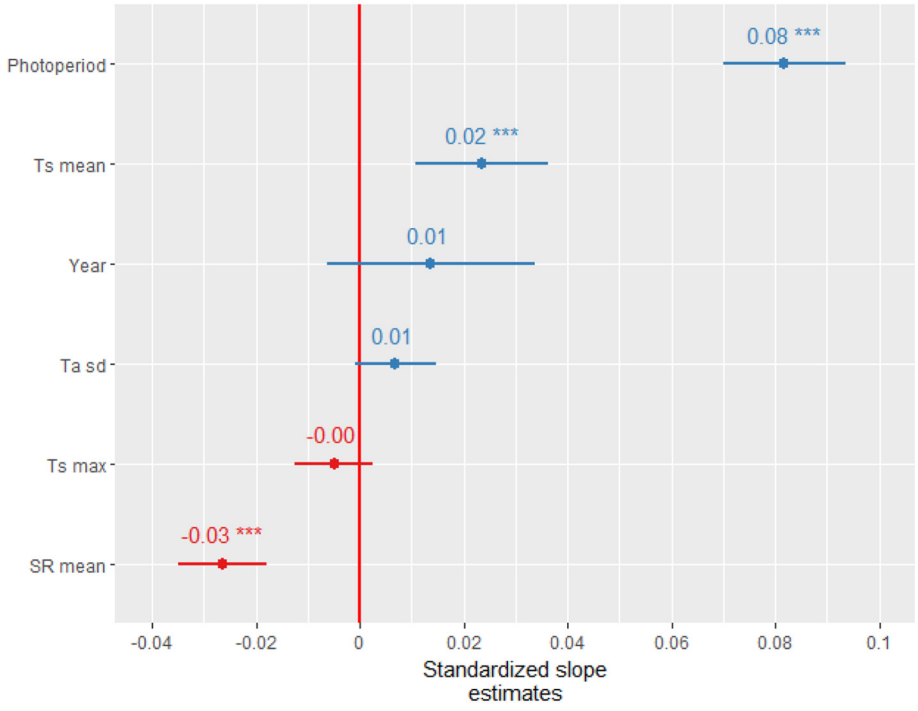

Fig. 5. Standardized slope (b*) estimates for predictor variables of the linear mixed effects model with PRI_0 as the dependent variable and the following fixed effects: Photoperiod, mean soil temperature (Ts_{mean}), standard deviation of air temperature (Ta_{sd}), maximum soil temperature (Ts_{max}), and mean solar radiation (SR_{mean}). Statistically significant ($p < 0.001$) fixed effects are marked with ***.

and temperature on the photosynthetic apparatus (Rosenthal and Camm, 1997; Busch et al., 2008; Stinziano and Way, 2014) and points towards the need to consider these interactions when interpreting late-season PRI_0 time-series in the context of climate change. For example, Rosenthal and Camm (1997) showed that increasing soil temperature and longer photoperiod both delayed foliar pigment changes in western larch (*Larix occidentalis*) during late-season senescence.

4.2. Suitability of late-season trends in PRI_0 for documenting climate change effects at northern treeline

Our results show clearly that photoperiod has by far the strongest effect on changes in PRI_0. However, the significant effect of SR_{mean} and Ts_{mean} on PRI_0 suggests that, theoretically, satellite-based time-series of PRI_0 from northern treeline sites could allow for understanding of climate change effects on photosynthetic phenology. For example, the linear mixed effects modeling results (Fig. 5) suggests that the ongoing warming and associated changes in cloud cover in the arctic region (Kattsov et al., 2005) should result in a more gradual decrease in PRI_0 during late-season, delaying the end of the growing season detected by PRI_0 time-series by several days. More specifically, the end of the growing season as detected by PRI_0 time-series would shift by almost a full week, by 6.41 ± 1.19 (mean and standard deviation) days based on predicted increases in Ts and decreasing SR_{mean} (Kattsov et al., 2005) by the end of the 21st century relative to observed seasonality in 2016. Such climate projections indicate possible increases in cloud cover that may decrease SR_{mean} by up to 10 $W\,m^{-2}$ and late-season Ta increases of 3–5 °C that may result in Ts_{mean} increases by 2 °C (Fig. 7). Even though the lack of reliable projections of Ta_{mean} and Ts_{mean} introduce uncertainties in the above scenario, it highlights the potential of PRI_0 time-series for understanding climate-change effects on the FTE.

However, the modeling results also suggest that care must be taken when interpreting PRI_0 time-series from FTE sites for two main reasons; first, the relative strength of standardized effects suggest that seasonally varying factors on PRI_0 are relatively small, so that even minor noise introduced by other factors - such as diurnal variability in xanthophyll-cycle pigments, viewing geometry, and snow cover - might obscure a signal (Ulsig et al., 2017; Middleton et al., 2016). In this study, we removed observations with snow on the ground from the analysis and we calculated PRI_0 to minimize effects due to variability in diurnal xanthophyll-cycle pigment interconversion and viewing geometry, but accounting for these factors when using satellite data will be more challenging. For example, Middleton et al. (2016) showed that time of day variations in satellite-derived PRI from Canadian forests in late morning (from MODIS Terra) or early afternoon (from MODIS Aqua) needed to be considred to correctly track LUE determined from flux towers. When using satellite imagery, it might be beneficial to focus the analysis on morning imagery (e.g., from MODIS Terra) before the light stress-induced onset of xanthophyll pigment interconversions. Further, to reduce BRDF effects, it could be useful to focus the analysis only on certain sensor geometries (e.g., forward scatter view) as opposed to including all available sensor geometries (forward scatter, nadir, and back scatter) (Middleton et al., 2016).

Second, our modeling results suggest that light availability (i.e., photoperiod and SR_{mean}) has by far the strongest effect on PRI_0 as oppose to Ts and Ta. This is problematic from a passive remote sensing perspective since cloud cover is expected to increase with climate change (Kattsov et al., 2005) and satellite measurements rely on clear days for data acquisitions, so that PRI time-series products may be biased towards years with clear skies and high SR_{mean} observations, ultimately resulting in misleading trends that may diverge from the actual trends associated with cloudier, low SR_{mean} years. Some initial research suggests that chlorophyll fluorescence from satellite remote sensing (e.g., NASA's OCO-2 or ESA's TROPOspheric Monitoring Instrument) could circumvent this problem since this approach is more robust to cloud conditions (e.g., Frankenberg and Berry, 2018) than reflectance-based approaches while providing comparable information about photosynthetic phenology. However, currently there are no longer-term (> 10 years) time-series of chlorophyll fluorescence data available and hence such longer-term analysis based on fluorescence data is not yet possible.

4.3. Additional considerations

The observational time-scale spans only two-years, whereas the effects of climate change act on a much longer temporal scale, potentially affecting the complex interaction between environmental and genetic factors. For example, over longer time-scales, increased warming might

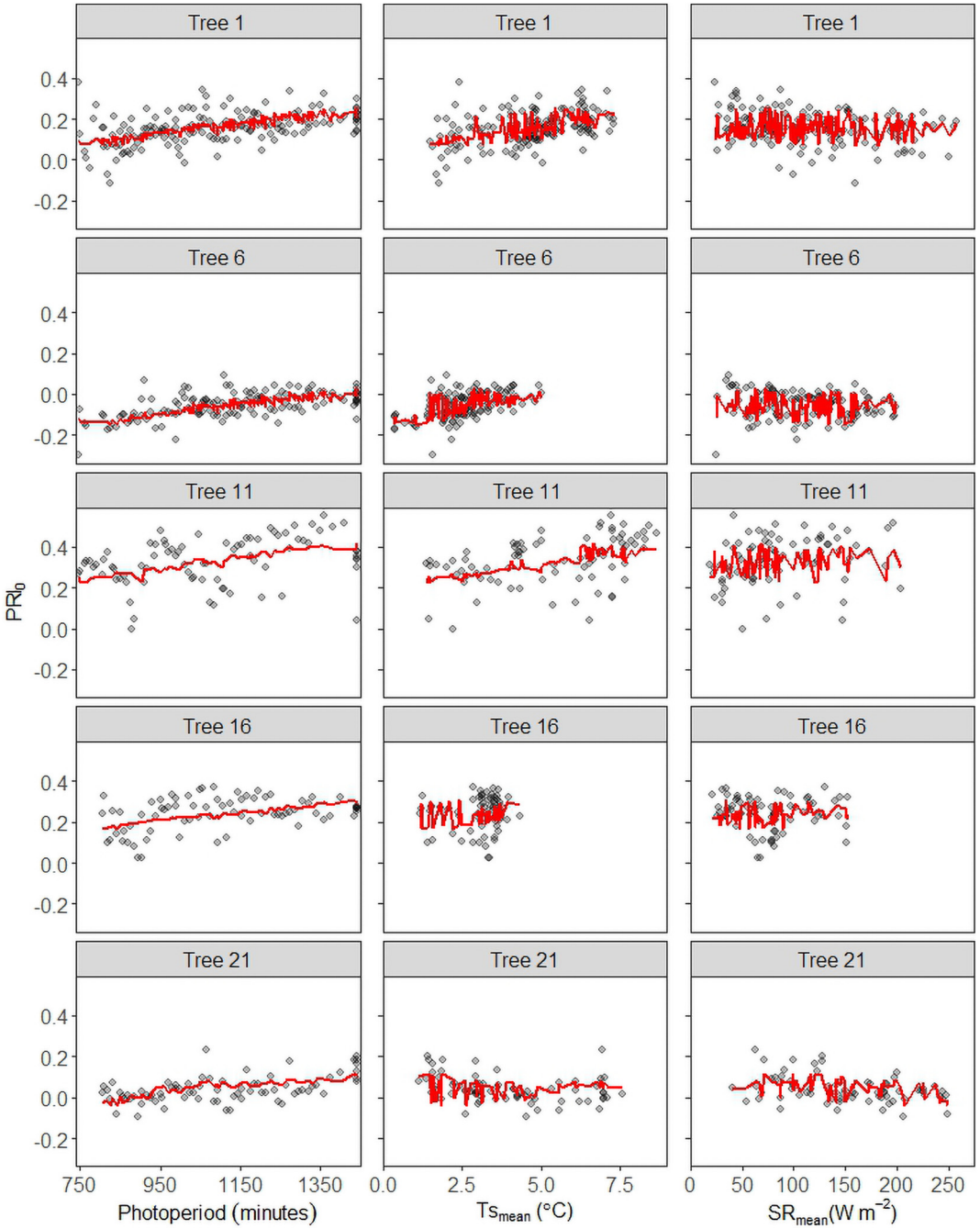

Fig. 6. Plots of the observed (points) and predicted values (red lines) for the three most important covariates (columns) - photoperiod, mean soil temperature (Ts_{mean}), and mean solar radiation (SR_{mean}) - across the complete time-series for five sampled trees (tree 1, 6, 11, 16, and 21, respectively). Predicted values were derived from the complete time series for each tree (5-min interval data) using a linear mixed effects model from an evaluation of drivers of PRI_0. Models were fitted using standardized covariates, but covariates are shown on their natural scales to improve interpretability. (For interpretation of the references to colour in this figure legend, the reader is referred to the web version of this article.)

facilitate evolutionary selection of trees where changes in PRI_0 are increasingly driven by Ta rather than photoperiod such that trees can take advantage of higher Ta for increased carbon gain which in turn would affect the interpretation of late-season PRI timeseries from the FTE (Körner, 2012; Körner et al., 2016; Stinziano and Way, 2017; Malcolm and Pymar, 1975). There is also evidence that environmental conditions during embryogenesis affects the timing of phenological events allowing trees to adapt their phenology to a changing climate from one generation to the next (Skrøppa et al., 2010; Yakovlev et al., 2010). Futher, this study focuses on late-season phenology, but to fully determine the suitability of PRI time-series for climate change research along the FTE, future work needs to evaluate how environmental factors drive changes in PRI during springtime – the season on which some pioneering PRI time-series work has been focused (e.g., Wong and Gamon, 2015b). The results from such work might show pronounced differences from results presented here since the timing of phenological events in the spring may be less driven by photoperiod and more by temperature when compared to the late-season (Körner, 2012). Having more certainty regarding drivers of PRI changes during spring could help to greatly improve the interpretation of early season PRI time-series in the context of climate change. Moreover, even though this study focuses on *Picea glauca*, an important northern treeline species in

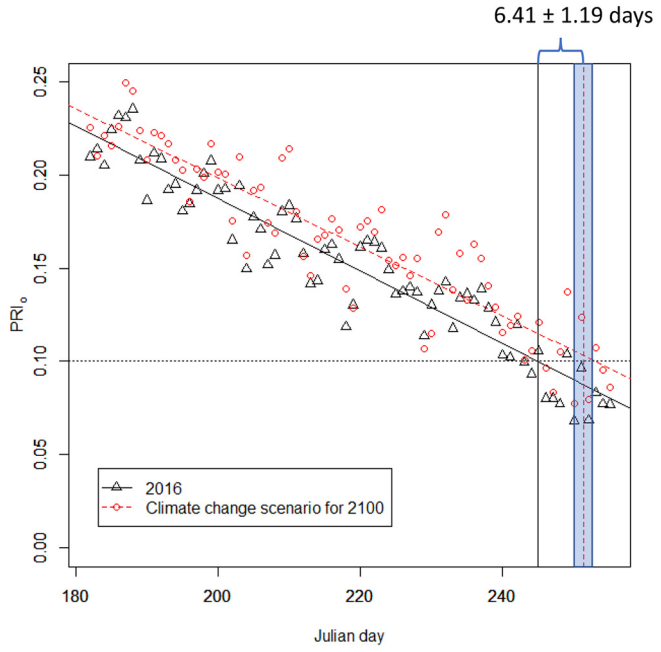

Fig. 7. Estimates of PRI_0 for a select tree for 2016 (black triangles) and 2100 (red circles). Estimates are based on the linear mixed effects model (see Fig. 5 for standardized slope estimates) that was used in predictive mode. Observed Ts_{mean} and SR_{mean} were used to parameterize the 2016 model. To parameterize the 2100 model, the following projections were used (Kattsov et al., 2005): increasing cloud cover that may result in decreasing SR_{mean} by up to 10 W m^{-2} and late-season Ta increases of 3–5 °C that may result in Ts_{mean} increases by 2 °C. The projected changes in means were randomly sampled from a normal distribution with a mean of 10 W m^{-2} (for SR_{mean}) and 2 °C (for Ts_{mean}) and added to the observed 2016 values. The random sampling was repeated 1000 times to yield an average (vertical dashed red line) and standard deviation (area shaded in blue) of the PRI_0 time-series shift. Julian day estimate when PRI_0 values reach an arbitrarily chosen late-season PRI_0 value of 0.10 (horizontal dashed black line) are marked for 2016 by a vertical black line and for 2100 by a vertical dashed red line. (For interpretation of the references to colour in this figure legend, the reader is referred to the web version of this article.)

North America, there may be species specific differences of how phenology responds to seasonal changes in environmental factors and to what degree (Silim and Lavender, 1994; Tanino et al., 2010; Cooke et al., 2012). Also, this study does not consider moisture dynamics which may control phenology (Silim and Lavender, 1994) and are expected to shift as a consequence of climate change (Kattsov et al., 2005). Moreover, PRI_0 was calculated using the PRI center wavelength of the SRS sensors at 532 nm as opposed to 531 nm (Gamon et al., 1992). This could contribute to the observed error structure (Fig. S1 in Supp. data) that might be slightly different to the error structure that would have been observed with a center wavelength at 531 nm. Lastly, PRI_0 was used here to minimize confounding effects of variations in xanthophyll cycle pigments driven by diurnal variation in radiation intensity and BRDF on late-seasonal PRI trends. However, when relying on satellite derived PRI readings acquired during the midday period, PRI_0 cannot be calculated and hence other correction approaches will be needed to account for these confounding effects. Despite the above listed limitations, this study provides initial evidence that late-season PRI time-series at the FTE are strongly driven by photoperiod but modulated by weather conditions that are anticipated to shift within a changing climate (e.g., Kattsov et al., 2005). These insights could advance our ability to interpret temporal dynamics in late-season PRI time-series for FTE sites in North America and Europe in the context of climate-change.

5. Conclusion

The results from this study provide novel insights on how to interpret late-season PRI time-series at the FTE in the context of climate change. Photoperiod, unaffected by environmental change, exhibited decidedly the strongest effect on PRI_0 partly supporting our hypothesis that photoperiod is the predominant driver of the PRI_0 signal at the FTE. However, environmental variables SR_{mean} and Ts_{mean}, both of which are expected to shift with a changing climate, also exhibited statistically significant, albeit weaker, effects on PRI_0. This suggests that PRI time-series may be a suitable tool for understanding climate change effects at the FTE with two important caveats: (1) the effects of environmental variables that are affected by climate change on the PRI_0 signal is relatively small ($b^* = 0.05$) when compared to photoperiod ($b^* = 0.08$) requiring rigorous approaches that account for potential noise from factors such as snow cover and viewing geometry; (2) variance in light environment (i.e., photoperiod and SR) exhibited the strongest effect on PRI_0 signal though the effect of variable lighting conditions on photosynthetic phenology may not be fully captured by PRI time-series since they rely on cloud free imagery that are projected to become less frequent with climate change, thereby biasing recorded PRI observations towards infrequent and higher light intensity collections.

Supplementary data to this article can be found online at https://doi.org/10.1016/j.rse.2018.11.022.

Acknowledgments

The funding for this work came from NASA Above grant NNX15AT86A. We thank Sarah Sackett and Jyoti Jennewein for their help with some of our fieldwork and logistical support. We would also like to thank Steven Garrity for some helpful discussions and advice. Lastly, we would like to thank three anonymous reviewers and associate editor Dr. John Gamon for their helpful comments and feedback that greatly improved the quality of the manuscript.

References

Adams, W.W., Demmig-Adams, B., 1994. Carotenoid composition and down regulation of photosystem II in three conifer species during the winter. Physiol. Plant. 92, 451–458.
Adams, W.W., Demmig-Adams, B., 1995. The xanthophyll cycle and sustained thermal energy dissipation activity in *Vinca minor* and *Euonymus kiautschovicus* in winter. Plant Cell Environ. 18, 117–127.
Adams, W.W., Demmig-Adams, B., Rosenstiel, T.N., Brightwell, A.K., Ebbert, V., 2002. Photosynthesis and photoprotection in overwintering plants. Plant Biol. 4, 545–557.
Adams, W.W., Zarter, C.R., Ebbert, V., Demmig-Adams, B., 2004. Photoprotective strategies of overwintering evergreens. AIBS Bull. 54, 41–49.
Akaike, H., 1974. A new look at the statistical model identification. IEEE Trans. Autom. Control 19 (6), 716–723. https://doi.org/10.1109/TAC.1974.1100705. (MR 0423716).
Boelman, N.T., Magney, T.S., Logan, B.A., Griffin, K.L., Eitel, J.U.H., Greaves, H., Prager, C.M., Vierling, L.A., 2016. Spectral determination of concentrations of functionally diverse pigments in increasingly complex arctic tundra canopies. Oecologia 182, 85–97.
Bowling, D.R., Logan, B.A., Hufkens, K., Aubrecht, D.M., Richardson, A.D., Burns, S.P., Anderegg, W.R.L., Blanken, P.D., Eiriksson, D.P., 2018. Limitations to winter and spring photosynthesis of a Rocky Mountain subalpine forest. Agric. For. Meteorol. 252, 241–255. https://doi.org/10.1016/j.agrformet.2018.01.025.
Busch, F., Huner, N.P.A., Ensminger, I., 2008. Increased air temperature during simulated autumn conditions impairs photosynthetic electron transport between photosystem II and photosystem I. Plant Physiol. 147, 402–414. https://doi.org/10.1104/pp.108.117598.
Callaghan, T.V., Werkman, B.R., Crawford, R.M., 2002. The tundra-taiga Interface and its dynamics: concepts and applications. AMBIO J. Hum. Environ. 12, 6–14.
Cooke, J.E.K., Eriksson, M.E., Juntilla, O., 2012. The dynamic nature of bud dormancy in trees: environmental control and molecular mechanisms. Plant Cell Environ. 35, 1707–1728. https://doi.org/10.1111/j.1365-3040.2012.02552.x.
Corripio, J.G., 2014. Insol: Solar Radiation. R Packag. Version 1, 2014.
Demmig-Adams, B., Adams III, W.W., 1992. Photoprotection and other responses of plants to high light stress. Annu. Rev. Plant Biol. 43, 599–626.
Dormling, I., Gustafsson, Å., von Wettstein, D., 1968. The experimental control of the life cycle in *Picea abies* (L.) Karst. Some basic experiments on the vegetative cycle. Silvae Genet. 17, 44–64.
Eitel, J.U.H., Vierling, L.A., Litvak, M.E., Long, D.S., Schulthess, U., Ager, A.A., Krofcheck,

D.J., Stoscheck, L., 2011. Broadband, red-edge information from satellites improves early stress detection in a New Mexico conifer woodland. Remote Sens. Environ. 115, 3640–3646.
Ensminger, I., Yao-Yun Chang, C., Bräutigam, K., 2015. Tree responses to environmental cues. Adv. Bot. Res. 74, 229–263. https://doi.org/10.1016/bs.abr.2015.05.003.
Filella, I., Porcar-Castell, A., Munné-Bosch, S., Bäck, J., Garbulsky, M.F., Peñuelas, J., 2009. PRI assessment of long-term changes in carotenoids/chlorophyll ratio and short-term changes in de-epoxidation state of the xanthophyll cycle. Int. J. Remote Sens. 30, 4443–4455. https://doi.org/10.1080/01431160802575661.
Frankenberg, C., Berry, J., 2018. Solar Induced Chlorophyll Fluorescence: Origins, Relation to Photosynthesis and Retrieval. pp. 143–162.
Fréchette, E., Chang, C.Y.Y., Ensminger, I., 2016. Photoperiod and temperature constraints on the relationship between the photochemical reflectance index and the light use efficiency of photosynthesis in *Pinus strobus*. Tree Physiol. 36, 311–324. https://doi.org/10.1093/treephys/tpv143.
Gamon, J.A., Penuelas, J., Field, C.B., 1992. A narrow-waveband spectral index that tracks diurnal changes in photosynthetic efficiency. Remote Sens. Environ. 41, 35–44.
Gamon, J.A., Field, C.B., Goulden, M.L., Griffin, K.L., Hartley, A.E., Joel, G., Penuelas, J., Valentini, R., 1995. Relationships between NDVI, canopy structure, and photosynthesis in three Californian vegetation types. Ecol. Appl. 5 (1), 28–41.
Gamon, J.A., Serrano, L., Surfus, J.S., 1997. The photochemical reflectance index: an optical indicator of photosynthetic radiation use efficiency across species, functional types, and nutrient levels. Oecologia 112, 492–501.
Gamon, J.A., Kovalchuck, O., Wong, C.Y.S., Harris, A., Garrity, S.R., 2015. Monitoring seasonal and diurnal changes in photosynthetic pigments with automated PRI and NDVI sensors. Biogeosciences 12, 4149–4159. https://doi.org/10.5194/bg-12-4149-2015.
Gamon, J.A., Huemmrich, K.F., Wong, C.Y.S., Ensminger, I., Garrity, S., Hollinger, D.Y., Noormets, A., Peñuelas, J., 2016. A remotely sensed pigment index reveals photosynthetic phenology in evergreen conifers. Proc. Natl. Acad. Sci. 113, 13087–13092. https://doi.org/10.1073/pnas.1606162113.
Garbulsky, M.F., Peñuelas, J., Gamon, J., Inoue, Y., Filella, I., 2011. The photochemical reflectance index (PRI) and the remote sensing of leaf, canopy and ecosystem radiation use efficiencies: a review and meta-analysis. Remote Sens. Environ. 115 (2), 281–297.
Garrity, S.R., Vierling, L.A., Bickford, K., 2010. A simple filtered photodiode instrument for continuous measurement of narrowband NDVI and PRI over vegetated canopies. Agric. For. Meteorol. 150 (3), 489–496.
Garrity, S.R., Eitel, J.U., Vierling, L.A., 2011. Disentangling the relationships between plant pigments and the photochemical reflectance index reveals a new approach for remote estimation of carotenoid content. Remote Sens. Environ. 115 (2), 628–635.
Gelman, A., 2008. Scaling regression inputs by dividing by two standard deviations. Stat. Med. 27, 2865–2873.
Harding, R., Kuhry, P., Christensen, T.R., Sykes, M.T., Dankers, R., van der Linden, S., 2002. Climate feedbacks at the tundra-taiga interface. AMBIO J. Hum. Environ. 12, 47–55.
Heide, O.M., 1974. Growth and dormancy in Norway spruce ecotypes (*Picea abies*) I. Interaction of photoperiod and temperature. Physiol. Plant. 1–12.
Howe, G.T., Aitken, S.N., Neale, D.B., Jermstad, K.D., Wheeler, N.C., Chen, T.H., 2003. From genotype to phenotype: unraveling the complexities of cold adaptation in forest trees. Can. J. Bot. 81, 1247–1266. https://doi.org/10.1139/b03-141.
Jeong, S.J., Ho, C.H., Gim, H.J., Brown, M.E., 2011. Phenology shifts at start vs. end of growing season in temperate vegetation over the Northern Hemisphere for the period 1982–2008. Glob. Chang. Biol. 17, 2385–2399. https://doi.org/10.1111/j.1365-2486.2011.02397.x.
Kattsov, V.M., Källén, E., Cattle, H., Christensen, J., Drange, H., Hanssen-bauer, I., Jóhannesen, T., Karol, I., Räisänen, J., Svensson, G., Chen, D., Polyakov, I., Rinke, A., 2005. Ch.04. Future Climate Change: Modeling and Scenarios for the Arctic Lead Authors. Arct. Clim. Impact Assess. pp. 99–150.
Körner, C., 2012. Alpine Treelines: Functional Ecology of the Global High Elevation Tree Limits. Springer Science & Business Media.
Körner, C., Basler, D., Hoch, G., Kollas, C., Lenz, A., Randin, C.F., Vitasse, Y., Zimmermann, N.E., 2016. Where, why and how? Explaining the low-temperature range limits of temperate tree species. J. Ecol. 104, 1076–1088. https://doi.org/10.1111/1365-2745.12574.
Lichtenthaler, H., 1987. Chlorophylls and carotenoids: pigments of photosynthetic biomembranes. Methods Enzymol. 148C, 350–382. https://doi.org/10.1016/0076-6879(87)48036-1.
Lüdecke, D., 2018. sjPlot: Data Visualization for Statistics in Social Science.
Lyapustin, A., Wang, Y., Korkin, S., Huang, D., n.d. MODIS Collection 6 MAIAC Algorithm.
Magney, T.S., Vierling, L.A., Eitel, J.U.H., Huggins, D.R., Garrity, S.R., 2016. Response of high frequency photochemical reflectance index (PRI) measurements to environmental conditions in wheat. Remote Sens. Environ. 173, 84–97.
Malcolm, D.C., Pymar, C.F., 1975. The Influence of Temperature on the Cessation of Height Growth of Sitka Spruce (*Picea sitchensis* (Bong.) Carr.) provenances.pdf.
Middleton, E.M., Cheng, Y.B., Hilker, T., Black, T.A., Krishnan, P., Coops, N.C., Huemmrich, K.F., 2009. Linking foliage spectral responses to canopy-level ecosystem photosynthetic light-use efficiency at a Douglas-fir forest in Canada. Can. J. Remote. Sens. 35 (2), 166–188.
Middleton, E.M., Huemmrich, K.F., Landis, D.R., Black, T.A., Barr, A.G., McCaughey, J.H., 2016. Photosynthetic efficiency of northern forest ecosystems using a MODIS-derived photochemical reflectance index (PRI). Remote Sens. Environ. 187, 345–366. https://doi.org/10.1016/j.rse.2016.10.021.
Niinemets, Ü., Kollist, H., García-Plazaola, J.I., Hernández, A., Becerril, J.M., 2003. Do the capacity and kinetics for modification of xanthophyll cycle pool size depend on growth irradiance in temperate trees? Plant Cell Environ. 26, 1787–1801. https://doi.org/10.1046/j.1365-3040.2003.01096.x.
Park, T., Ganguly, S., Tømmervik, H., Euskirchen, E.S., Høgda, K.A., Karlsen, S.R., Brovkin, V., Nemani, R.R., Myneni, R.B., 2016. Changes in growing season duration and productivity of northern vegetation inferred from long-term remote sensing data. Environ. Res. Lett. 11. https://doi.org/10.1088/1748-9326/11/8/084001.
Piao, S., Wang, X., Ciais, P., Zhu, B., Wang, T.A.O., Liu, J.I.E., 2011. Changes in satellite-derived vegetation growth trend in temperate and boreal Eurasia from 1982 to 2006. Glob. Chang. Biol. 17 (10), 3228–3239.
Pinheiro, J., Bates, D., DebRoy, S., Sarkar, D., R Core Team, 2017. {nlme}: Linear and Nonlinear Mixed Effects Models.
Porcar-Castell, A., Garcia-Plazaola, J.I., Nichol, C.J., Kolari, P., Olascoaga, B., Kuusinen, N., Fernández-Marín, B., Pulkkinen, M., Juurola, E., Nikinmaa, E., 2012. Physiology of the seasonal relationship between the photochemical reflectance index and photosynthetic light use efficiency. Oecologia 170, 313–323.
R Core Team, 2017. R: A language and environment for statistical computing. R Foundation for Statistical Computing, Vienna, Austria. https://www.R-project.org/.
Ramankutty, N., Foley, J.A., Norman, J., McSweeney, K., 2002. The global distribution of cultivable lands: current patterns and sensitivity to possible climate change. Glob. Ecol. Biogeogr. 11, 377–392.
Reed, B.C., Brown, J.F., VanderZee, D., Loveland, T.R., Merchant, J.W., Ohlen, D.O., 1994. Measuring phenological variability from satellite imagery. J. Veg. Sci. 5 (5), 703–714.
Rosenthal, S.I., Camm, E.L., 1997. Photosynthetic decline and pigment loss during autumn foliar senescence in western larch (*Larix occidentalis*). Tree Physiol. 17, 767–775. https://doi.org/10.1093/treephys/17.12.767.
Salisbury, F.B., 1981. Responses to photoperiod. In: Physiological Plant Ecology I. Springer, pp. 135–167.
Schielzeth, H., 2010. Simple means to improve the interpretability of regression coefficients. Methods Ecol. Evol. 1, 103–113. https://doi.org/10.1111/j.2041-210X.2010.00012.x.
Serreze, M.C., Walsh, J.E., Chapin, F.S., Osterkamp, T., Dyurgerov, M., Romanovsky, V., Oechel, W.C., Morison, J., Zhang, T., Barry, R.G., 2000. Observational evidence of recent change in the northern high-latitude environment. Clim. Chang. 46, 159–207.
Silim, S.N., Lavender, D.P., 1994. Seasonal patterns and environmental regulation of frost hardiness in shoots of seedlings of *Thuja plicata*, *Chamaecyparis nootkatensis*, and *Picea glauca*. Can. J. Bot. 72, 309–316. https://doi.org/10.1139/b94-040.
Skre, O., Baxter, R., Crawford, R.M.M., Callaghan, T.V., Fedorkov, A., 2002. How will the tundra-taiga interface respond to climate change? AMBIO J. Hum. Environ. 12, 37–46.
Skrøppa, T., Tollefsrud, M.M., Sperisen, C., Johnsen, Ø., 2010. Rapid change in adaptive performance from one generation to the next in *Picea abies* - Central European trees in a Nordic environment. Tree Genet. Genomes 6, 93–99.
Sofronova, V.E., Dymova, O.V., Golovko, T.K., Chepalov, V.A., Petrov, K.A., 2016. Adaptive changes in pigment complex of *Pinus sylvestris* needles upon cold acclimation. Russ. J. Plant Physiol. 63, 433–442. https://doi.org/10.1134/S1021443716040142.
Stinziano, J.R., Way, D.A., 2014. Combined effects of rising [CO_2] and temperature on boreal forests: growth, physiology and limitations[1]. Botany 92, 425–436. https://doi.org/10.1139/cjb-2013-0314.
Stinziano, J.R., Way, D.A., 2017. Autumn photosynthetic decline and growth cessation in seedlings of white spruce are decoupled under warming and photoperiod manipulations. Plant Cell Environ. 40, 1296–1316. https://doi.org/10.1111/pce.12917.
Sykes, M.T., Prentice, I.C., Cramer, W., 1996. A bioclimatic model for the potential distributions of north European tree species under present and future climates. J. Biogeogr. 203–233.
Tang, J., Körner, C., Muraoka, H., Piao, S., Shen, M., Thackeray, S.J., Yang, X., 2016. Emerging opportunities and challenges in phenology: a review. Ecosphere 7 (8).
Tanino, K.K., Kalcsits, L., Silim, S., Kendall, E., Gray, G.R., 2010. Temperature-driven plasticity in growth cessation and dormancy development in deciduous woody plants: a working hypothesis suggesting how molecular and cellular function is affected by temperature during dormancy induction. Plant Mol. Biol. 73, 49–65. https://doi.org/10.1007/s11103-010-9610-y.
Thomas, B., Vince-Prue, D., 1997. Photoperiodic control of flower initiation: some general principles. In: Photoperiod. Plants, pp. 3–28.
Tranquillini, W., 1979. Physiological Ecology of the Alpine Timberline: Tree Existence at High Altitudes with Special Reference to the European Alps. Springer Science & Business Media.
Ulsig, L., Nichol, C.J., Huemmrich, K.F., Landis, D.R., Middleton, E.M., Lyapustin, A.I., Mammarella, I., Levula, J., Porcar-Castell, A., 2017. Detecting inter-annual variations in the phenology of evergreen conifers using long-term MODIS vegetation index time-series. Remote Sens. 9. https://doi.org/10.3390/rs9010049.
Vaartaja, O., 1954. Photoperiodic ecotypes of trees. Can. J. Bot. 32, 392–399.
Verhoeven, A., 2014. Sustained energy dissipation in winter evergreens. New Phytol. 201, 57–65. https://doi.org/10.1111/nph.12466.
Wang, X., Piao, S., Xu, X., Ciais, P., Macbean, N., Myneni, R.B., Li, L., 2015. Has the advancing onset of spring vegetation green-up slowed down or changed abruptly over the last three decades? Glob. Ecol. Biogeogr. 24, 621–631. https://doi.org/10.1111/geb.12289.
Wong, C.Y.S., Gamon, J.A., 2015a. Three causes of variation in the photochemical reflectance index (PRI) in evergreen conifers. New Phytol. 206, 187–195. https://doi.org/10.1111/nph.13159.
Wong, C.Y.S., Gamon, J.A., 2015b. The photochemical reflectance index provides an optical indicator of spring photosynthetic activation in evergreen conifers. New Phytol. 206, 196–208. https://doi.org/10.1111/nph.13251.

Yakovlev, I.A., Fossdal, C.G., Johnsen, Ø., 2010. MicroRNAs, the epigenetic memory and climatic adaptation in Norway spruce. New Phytol. 187, 1154–1169. https://doi.org/10.1111/j.1469-8137.2010.03341.x.

Zeng, H., Jia, G., Epstein, H., 2011. Recent changes in phenology over the northern high latitudes detected from multi-satellite data. Environ. Res. Lett. 6, 045508. https://doi.org/10.1088/1748-9326/6/4/045508.

Zhang, W., Miller, P.A., Smith, B., Wania, R., Koenigk, T., Döscher, R., 2013. Tundra shrubification and tree-line advance amplify arctic climate warming: results from an individual-based dynamic vegetation model. Environ. Res. Lett. 8, 034023. https://doi.org/10.1088/1748-9326/8/3/034023.

Zuur, A.F., Ieno, E.N., Elphick, C.S., 2010. A protocol for data exploration to avoid common statistical problems. Methods Ecol. Evol. 1, 3–14. https://doi.org/10.1111/j.2041-210X.2009.00001.x.